

Appl Nanosci (2015) 5:245–253  
DOI 10.1007/s13204-014-0313-6

## ORIGINAL ARTICLE

# Optical, electrochemical and thermal properties of $\text{Co}^{2+}$ -doped CdS nanoparticles using polyvinylpyrrolidone

S. Muruganandam · G. Anbalagan ·  
G. Murugadoss

Received: 10 January 2014 / Accepted: 23 April 2014 / Published online: 16 May 2014  
© The Author(s) 2014. This article is published with open access at Springerlink.com

**Abstract**  $\text{Co}^{2+}$  (1–5 and 10 %) -doped cadmium sulfide nanoparticles were synthesized by the chemical precipitation method using polyvinyl pyrrolidone (PVP) as a surfactant. The X-ray diffraction results showed that Co ions were successfully incorporated into the CdS lattice and the transmission electron microscopy results revealed that the synthesized particles were aligned as rod-like structures. The absorption spectra of all the prepared samples (undoped and doped) were significantly blue shifted (472–504 nm) from the bulk CdS (512 nm). However, the absorption spectra of the doped samples were red shifted (408–504 nm) with respect to the doping concentrations (1–5 and 10 %). Furthermore, a dramatic blue shift absorption is observed at 472 nm for PVP-capped  $\text{CdS}:\text{Co}^{2+}$  (4 %) nanoparticles. In the photoluminescence study, two emission peaks were dominated in the green region at 529 and 545 nm corresponding the  $\text{CdS}:\text{Co}^{2+}$  nanoparticles. By correlating optical and EPR spectral data, the site symmetry of  $\text{Co}^{2+}$  ion in the host lattice was determined as both octahedral and tetrahedral. The presence of functional groups in the synthesized nanoparticles was identified by Fourier transform infrared spectroscopy. The thermal stability of the Co ions in CdS nanoparticles was studied by TG–DTA. In addition, an electrochemical property of the undoped and doped samples was studied by cyclic voltammetry for electrode applications.

**Keywords**  $\text{CdS}:\text{Co}^{2+}$  · Nanoparticles · Photoluminescence · Cyclic voltammetry · EPR

## Introduction

In recent years, semiconductor nanoparticles exhibit specific properties due to the quantum confinement effects, as a consequence of their size in nanometric range and the special luminescent properties caused by widening the band gap when the spatial dimension is reduced (Brus 1986; Rossetti et al. 1985; Hu and Zhang 2006). Due to the quantum size effect, semiconductor nanoparticles, especially the II–VI semiconductor nanoparticles, exhibit size-dependent optical properties (Alivisatos 1996). CdS is an n-type semiconductor with a direct band gap of 2.4 eV. Cadmium sulfide can be used as sensitizers in quantum dot-sensitized solar cells. It also has application in nonlinear optics (Liu et al. 2004), light-emitting diodes (Gopal et al. 2009; Kar and Chaudhuri 2006), solar energy conversion (Weller 2003), thin film transistors (Duan et al. 2003), gas detectors (Afify and Battisha 2000), optoelectronics (Hikmet et al. 2003), photo catalysis (Huynh et al. 2002), photovoltaic cells (Uda et al. 1997), X-ray detectors (Frederichs 1950) and as a window material for hetero-junction solar cells because it has usually a high absorption coefficient (Oladeji et al. 2000). Doping with transition metal elements into CdS nanoparticles leads to many interests. Especially, transition metal doped with CdS nanoparticles with good crystal structural, electrical and optical properties has been reported. The optical and electrical properties of CdS are strongly modified by the doping of  $\text{Co}^{2+}$  because of the sp–d exchange interaction between the localized d electrons of the transition metal magnetic ions and the mobile carriers in the valance band or conduction

S. Muruganandam · G. Anbalagan (✉)  
Department of Physics, Presidency College,  
Chennai 600 005, India  
e-mail: anbu24663@yahoo.co.in

G. Murugadoss  
Centre for Nanoscience and Technology, Anna University,  
Chennai 600 025, India

band. Among the transition metallic elements,  $\text{Co}^{2+}$  is an important transition metal element. Because, the ion radius of  $\text{Co}^{2+}$  is smaller than that of  $\text{Cd}^{2+}$ , which means that  $\text{Co}^{2+}$  can easily penetrate into CdS crystal lattice or substitute  $\text{Cd}^{2+}$  position in crystal (Sathyamoorthy et al. 2010). Currently, tuning the optical absorption of the semiconductor compound by adding dopant is an important issue. In this regard we have successfully doped the Co ions into the CdS lattice for tuning their optical properties for solar cell applications. Further, we tuned the optical absorption of the doped nanoparticles by introducing with different concentrations of the  $\text{Co}^{2+}$  (1–5, 10 %).

Chemical precipitation method is one of the most popular techniques that are used in industrial applications because of the cheap raw materials, easy handling and large-scale production (Souici et al. 2006). Recently, several methods have been developed to cap the surfaces of the nanoparticles with organic or inorganic groups, so that the nanoparticles not only are stable against agglomeration but also improve some optical properties of the nanoparticles. Some particular passivators used as PVA (Khanna et al. 2005), PAN (Meng et al. 2000), PVP (Wang et al. 2005a, b), and PAA (Xiao et al. 2001) have been investigated. In this research work, polyvinyl pyrrolidone (PVP) is used as a capping agent for synthesis of the Co-doped CdS nanoparticles by chemical method. The polymers may be a good choice as stabilizers as they can interact with the metal ions by complex or ion-pair formation and can be designed for certain physical properties of semiconductor nanoparticles (Murugadoss 2010).

## Experimental

### Materials

Cadmium acetate ( $\text{Cd}(\text{CH}_3\text{COO})_2 \cdot 2\text{H}_2\text{O}$ ), cobalt acetate ( $\text{Co}(\text{CH}_3\text{COO})_2 \cdot 4\text{H}_2\text{O}$ ) and sodium sulfide ( $\text{Na}_2\text{S} \cdot x\text{H}_2\text{O}$ ) obtained from the Nice chemical company, India were used as precursors. Polyvinylpyrrolidone (PVP—40,000) was received from Aldrich. All chemicals were used as received. Ultrapure water and acetone were used for all dilution and sample preparation.

### Synthesis of Co-doped CdS nanoparticles

Cobalt-doped CdS nanoparticles have been synthesized by the aqueous chemical precipitation method. 0.1 M aqueous solution of cadmium acetate dihydrate ( $\text{Cd}(\text{CH}_3\text{COO})_2 \cdot 2\text{H}_2\text{O}$ ) and cobalt acetate tetrahydrate ( $\text{Co}(\text{CH}_3\text{COO})_2 \cdot 4\text{H}_2\text{O}$ ) was prepared with deionized water. These two solutions were mixed together and stirred magnetically at 80 °C until a homogeneous solution was

obtained. The 0.1 M of sodium sulfide ( $\text{Na}_2\text{S}$ ) solution was also prepared with deionized water with the precursor ratio of 1:1. After an hour, aqueous solution of  $\text{Na}_2\text{S}$  was added dropwise into the mixed solution of cadmium acetate and cobalt acetate at room temperature, which resulted in an orange yellowish solution of Co:CdS. The solution was then refluxed with constant stirring at 120 °C for 30 min to attain saturation, which contains Co:CdS nanoparticles. The solution, after attaining the room temperature was added with small quantities of acetone with stirring to precipitate the nanoparticles. It was dried in hot air oven at 80 °C for 2 h.  $\text{Co}^{2+}$ -doped CdS nanoparticles with six different  $\text{Co}^{2+}$  concentrations (1, 2, 3, 4, 5 and 10 %) were prepared by the same procedure. In addition, for synthesis of surfactant (PVP)-capped particles different amounts (0.5–2.5 g) of PVP were added in cadmium acetate solution before the addition of cobalt acetate.

### Techniques

The synthesized samples were then subjected to powder X-ray diffraction (XRD) analysis for structural characterization using X'pert PRO diffractometer with  $\text{CuK}_\alpha$  radiation ( $\lambda = 1.5406 \text{ \AA}$ ) in the range of 20°–60° (2 $\theta$ ) at a scanning rate of 0.05° min<sup>−1</sup>. The infrared spectra of the nanoparticles were recorded at room temperature using NICOLET AVATAR 3330 FT-IR spectrometer by employing a KBr pellet technique. Optical absorption was studied using a Cary 500 UV–Visible diffuse reflectance mode spectrophotometer and luminescence properties were studied by fluorescence spectroscopy using Cary-Eclipse spectrometer with Xenon lamp source of 450 W. Crystallinity and size of the synthesized samples were studied by transmission electron microscope using 100 kV HITACHI (Japan) H-7650. Electron spin resonance (ESR) spectrum of the  $\text{CdS}:\text{Co}^{2+}$  powder was measured on an EPR spectrometer (Bruker EMX Plus), (9.859 GHz/0.6325 mW) at room temperature. Electrochemical measurements were performed using a CHI 660D Biologic instrument. The electrochemical properties of undoped and Co-doped CdS nanoparticles were studied by cyclic voltammetry. Three electrode systems were used consisting of glassy carbon electrode (GCE) with geometric surface area 7.1 mm<sup>2</sup>, Ag/AgCl reference electrode ( $\text{Ag}/\text{AgCl}_3 \text{ mol L}^{-1} \text{ KCl}$ ) and Pt counter electrode. The working electrodes were prepared by coating a slurry containing a mixture of the active material (80 wt%), nafion<sup>®</sup> 117 solution (20 wt%). The coated mesh was dried at 80 °C in vacuum cabinet overnight. The Ag/AgCl electrode with CdS and  $\text{CdS}:\text{Co}$  nanoparticles grown on the surface was characterized by electrochemical measurements. Cyclic voltammetry (CV) measurements were carried out at a scan rate of 20 mV s<sup>−1</sup>. Thermal analysis including TGA and DTA

was carried out using a simultaneous thermal analyzer SDT Q600 V8.3 Build 101 at the heating rate of  $20\text{ }^{\circ}\text{C min}^{-1}$  in an air atmosphere.

## Results and discussion

### X-ray powder diffraction analysis

X-ray powder diffraction pattern of the synthesized nanoparticles (Fig. 1a–g) shows a perfect match with the cubic zinc blende phase of CdS (hawleyite) (JCPDS 10-454). The peaks can be indexed as (111), (220) and (311) which are characteristic peaks of crystal planes for CdS cubic phase. The diffraction pattern for (111) peak position shows a shift towards higher angle of  $2\theta$  (lower  $d$  value) with increasing cobalt concentration. This clearly implies the lattice compression and thus confirming the dopant incorporation in the synthesized CdS NPs (Hanif et al. 2002; Saravanan et al. 2011). Further the widths of the diffraction peaks are broadened indicating that the cobalt-doped CdS NPs has a nanoscale distribution. Upon doping, no additional reflections were observed up to 5 % Co doping indicating that the cubic phase of CdS structure is not disturbed by the cobalt substitution and there are no impurities present in the sample. However at 10 % of dopant concentration some extra peaks have been observed along with characteristic peaks. The presence of the new peaks at  $28.457$ ,  $29.829$  and  $35.824$  indicates the hexagonal structure of CdS (Greenockite, JCPDS Card No. 41-1049). It has been observed that the surface capping with PVP molecule does not have any effect on the crystal structure of CdS:Co<sup>2+</sup> nanorods. The average particle size was calculated using Scherrer formula (Jenkins and Snyder 1996):  $D_{\text{XRD}} = 0.9\lambda/(\beta\cos\theta)$  where  $D_{\text{XRD}}$  is the average crystalline size,  $\lambda$  is the wavelength of CuK $\alpha$ ,  $\beta$  is the full width at half maximum of the diffraction peak, and  $\theta$  is the Bragg's angle. The average particle size of uncapped CdS:Co<sup>2+</sup> (1–5 and 10 %) and PVP-capped CdS:Co<sup>2+</sup> (4 %) nanoparticles is found to be 7.3, 7.3, 7.8, 9.7, 11.9, 12.6 and 6.4 nm, respectively.

### Structural analysis

The morphology of the uncapped and PVP-capped CdS:Co<sup>2+</sup> (4 %) nanoparticle was studied by TEM techniques. TEM images of CdS:Co<sup>2+</sup> nanoparticles shown in Fig. 2a indicate that the particles are highly aggregated due to the absence of capping agent. The image of NPs establishes the reasonable uniformity of the particle size, with spherical shape with the average size of  $\sim 10$  nm, which agrees with the XRD data. Well-shaped nanorods of CdS:Co<sup>2+</sup> with PVP capped is shown in Fig. 2b, c. This is

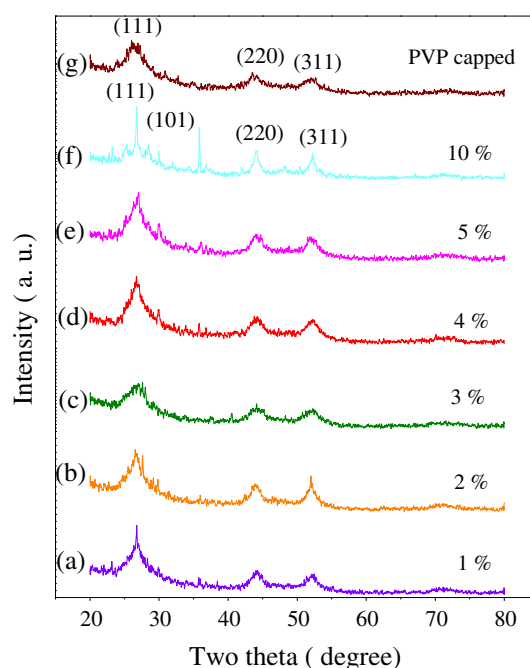


**Fig. 1** Powder X-ray diffraction patterns of Co<sup>2+</sup> CdS nanoparticles

may be due to the assembly of the smaller size nanoparticles (CdS:Co<sup>2+</sup>) by the carboxylic molecules (PVP). From the TEM photographs, one could find that PVP is not only controlling the particle size, but also assembling the particles as nanorods.

### FT-IR spectral analysis

FT-IR spectroscopy gives qualitative information about the way in which the adsorbed surfactant molecules are bound to the surface of CdS:Co<sup>2+</sup> nanoparticles. The room temperature FT-IR spectra of CdS:Co<sup>2+</sup> (4 %) and PVP-capped CdS:Co<sup>2+</sup> (4 %) nanoparticles recorded in the range of  $4,000\text{--}400\text{ cm}^{-1}$  is shown in Fig. 3. The absorption band observed between  $600$  and  $700\text{ cm}^{-1}$  is due to C–S stretching vibration (Martin and Schaber 1982; Sun et al. 2008). The absorption band appearing at  $927\text{ cm}^{-1}$  is assigned to S–O stretching vibration. The additional weak bands observed at  $2,343$  and  $1,638\text{ cm}^{-1}$  are due to microstructure formation of the sample. The absorption band occurring at  $1,110\text{ cm}^{-1}$  is due to the C–O stretching bands. Thus, the nanoparticles include a structure containing Cd–S and C–O in all samples Fig. 3a, b. A strong band present at  $1,412\text{ cm}^{-1}$  is due to stretching vibration of sulfite. The broad absorption band centered at  $3,429\text{ cm}^{-1}$  is attributed to the O–H stretching mode of H<sub>2</sub>O adsorbed on the surface of the samples. The weak and a strong absorption peak centered at  $2,360$  and  $1,560\text{ cm}^{-1}$  were attributed to CO<sub>2</sub> adsorbed on the surface of the particles. In fact, adsorbed water and CO<sub>2</sub> are common to all powder

**Fig. 2** SEM photograph of  $\text{Co}^{2+}$  doped (4 %):CdS and PVP capped  $\text{Co}^{2+}$  doped (4 %):CdS

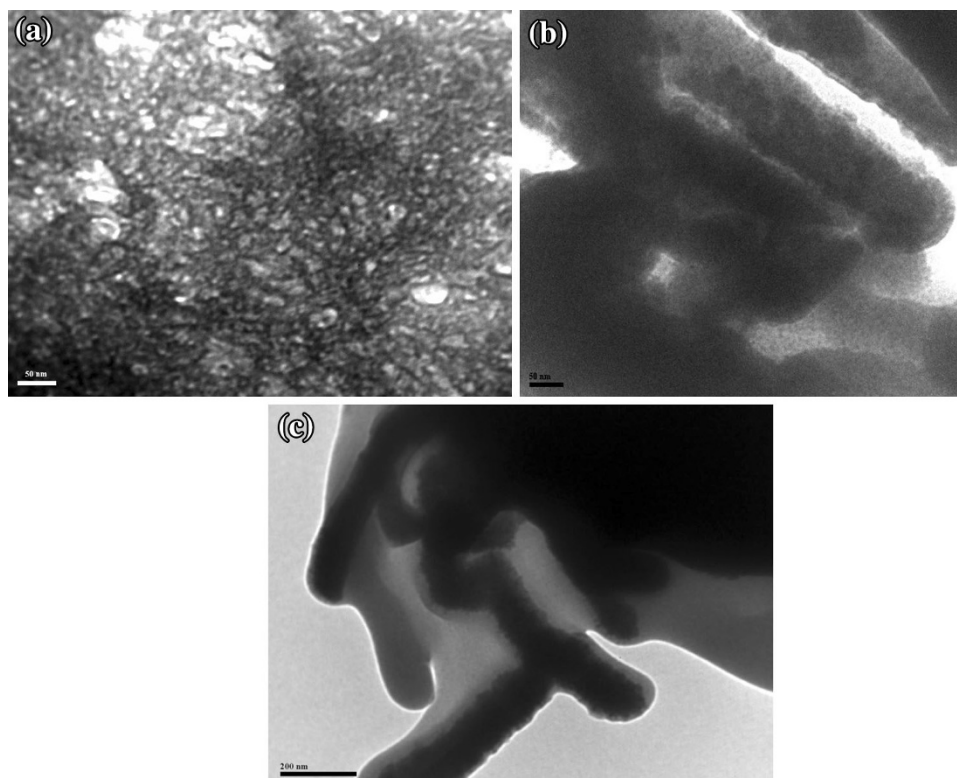
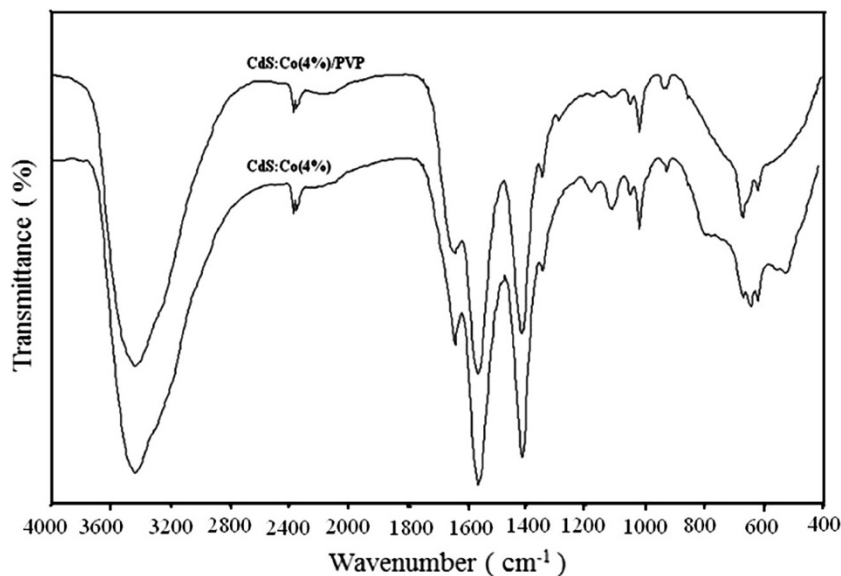


**Fig. 3** FT-IR spectrum shows the doped  $\text{CdS}:\text{Co}^{2+}$  (4 %) and  $\text{CdS}:\text{Co}/\text{PVP}$ -capped nanoparticles



samples exposed to the atmosphere and are more pronounced for nanosized particles with high surface area. The FT-IR spectra suggesting that doped CdS nanoparticles were prepared with a high degree of purity. The presence of absorption peak at  $1,290\text{ cm}^{-1}$  is due to C–O which was common in all the PVP-capped nanoparticles of the present study. This clearly confirms that the surface of  $\text{CdS}:\text{Co}^{2+}$  nanoparticles were capped by PVP.

#### UV–Visible absorption

The absorption spectra of  $\text{Co}^{2+}$  (1–5 and 10 %)-doped CdS and PVP-capped  $\text{CdS}:\text{Co}^{2+}$  nanoparticles in the range of 200–800 nm are presented in Fig. 4. The bands between 600 and 750 nm represent the tetrahedral coordination of  $\text{Co}^{2+}$  in CdS. Thus it can be concluded that  $\text{Co}^{2+}$  exists in a tetrahedral coordination. The presence of absorption band



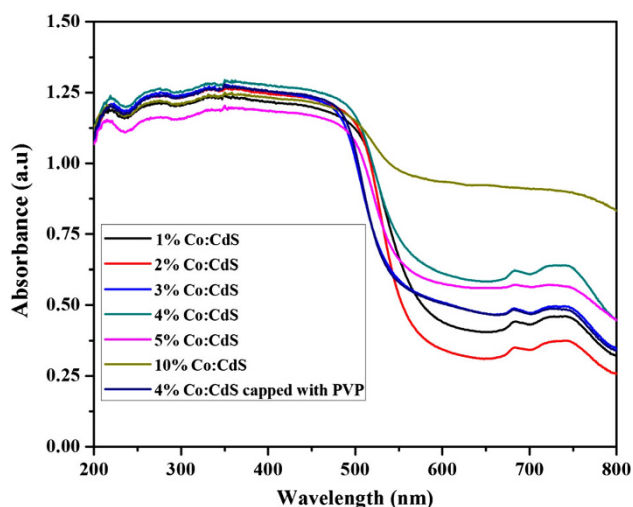


**Fig. 4** UV-Vis absorption spectra of CdS:Co  $\text{Co}^{2+}$  (1–5 and 10 %) and CdS:Co (4 %)/PVP-capped nanoparticles

around  $15,000 \text{ cm}^{-1}$  (684 nm) in the visible region corresponds to  $^4\text{A}_2(\text{F}) \rightarrow ^4\text{T}_1(\text{P})$  transition of tetrahedral coordination. The absorption bands in 200–350 nm wavelength range can be assigned to the  $\text{O}^{2-} \rightarrow \text{Co}^{2+}$  charge transfer process (He et al. 2005). The absorption values of the prepared samples were noticeably blue shifted from bulk CdS (520 nm). The shift in the band gap with size dominates the spectral changes (Nanda et al. 2000) because the binding energy of the exciton increases with decreasing size due to the increasing coulombic overlap enforced by spatial localization of the wave functions. This blue shift in the optical absorption edge indicates the formation of CdS particles in the nanometre region. This result is a direct consequence of the quantum confinement effect associated with smaller particle size. The estimated band gap values for  $\text{Co}^{2+}$  (1–5 and 10 %)-doped CdS and PVP-capped CdS:Co $^{2+}$  nanoparticles corresponding to the absorption edges are 480 nm (2.58 eV), 481 nm (2.58 eV), 484 nm (2.56 eV), 494 nm (2.51 eV), 501 nm (2.48 eV), 504 nm (2.46 eV), and 472 nm (2.63 eV), respectively, blue shifted compared with the absorption edge of the bulk CdS (512 nm).

The band gap of the nanoparticles ( $E_{\text{gn}}$ ) is calculated using relation  $E_{\text{gn}} = hc/\lambda$  and the calculated values given in Table 1. Brus (1984) showed that semiconductor nanoparticles with a particle radius significantly smaller than the exciton Bohr radius exhibit strong size-dependent optical properties due to the strong quantum confinement effect (QCE):

$$E_{\text{g}} = E_{\text{g}}^0 + \frac{h^2}{8\mu R^2} - \frac{1.8e^2}{4\pi \epsilon R}$$

where  $E_{\text{g}}^0$  is the energy band gap of the bulk material,  $R$  is the radius of the nanoparticle calculated from XRD data,

**Table 1** Energy gap, absorption and particle size with respect to the concentrations of  $\text{Co}^{2+}$

Doping concentration (wt%)	Band gap (eV)	Absorption wavelength (nm)	Particle size (nm)	
			UV data	PXRD data
CdS:Co $^{2+}$ (1 %)	2.46	504	7.3	7.3
CdS:Co $^{2+}$ (2 %)	2.48	501	7.3	7.3
CdS:Co $^{2+}$ (3 %)	2.51	494	7.8	7.8
CdS:Co $^{2+}$ (4 %)	2.56	484	9.7	9.7
CdS:Co $^{2+}$ (5 %)	2.58	481	11.9	11.9
CdS:Co $^{2+}$ (10 %)	2.58	480	14.6	12.6
CdS:Co $^{2+}$ (4 %)/PVP	2.63	472	6.5	6.4

$1/\mu = 1/m_e + 1/m_h$  ( $m_e$  and  $m_h$  being the electron and hole effective masses, respectively),  $\epsilon$  is the dielectric constant and  $e$  is the electronic charge. Here the electron effective mass ( $m_e$ ), hole effective mass ( $m_h$ ) and the dielectric constant ( $\epsilon$ ) for CdS are  $0.19 m_0$ ,  $0.8 m_0$  and  $5.7 \epsilon_0$ , respectively (Ohde et al. 2002). It is clear from Table 1 that there is a decrease in energy band gap values with an increase in cobalt concentration. This red shift of the energy band gap with increasing cobalt concentration is interpreted as mainly due to the sp–d exchange interactions between the band electrons and the localized d electrons of the  $\text{Co}^{2+}$  ions substituting host ions and is consistent with the reported results (Kumbhoikar et al. 2000), giving an additional evidence of cobalt substitution (Singhal et al. 2010). Also the calculated particle size of the uncapped and PVP-capped CdS:Co $^{2+}$  nanoparticles are in close agreement with the powder XRD result.

### Photoluminescence

Figure 5a, b shows the photoluminescence spectra of CdS:Co $^{2+}$  (4 %) and PVP-capped CdS:Co $^{2+}$  (4 %) nanoparticles. The peak position of all the photoluminescence (PL) spectra is nearly same. However, intensity is significantly changed. A maximum PL intensity has been observed at 4 % Co-doped CdS. Further by increasing the doping concentration from 5 to 10 %, the PL intensity is found to be decreased. It indicates that the 4 % of  $\text{Co}^{2+}$  is an optimum concentration for enhanced PL emission. The emission bands centered at 529 and 545 nm in green emission of  $\text{Co}^{2+}$ -doped CdS nanoparticles, respectively. The strong PL emission is due to the increased recombination of electrons trapped inside a sulfur vacancy with a hole in the valence band. The present study indicates that the luminescence properties of the capped CdS:Co $^{2+}$  nanoparticles have been attributed to the surface passivation of the nanoparticles with PVP, which can also

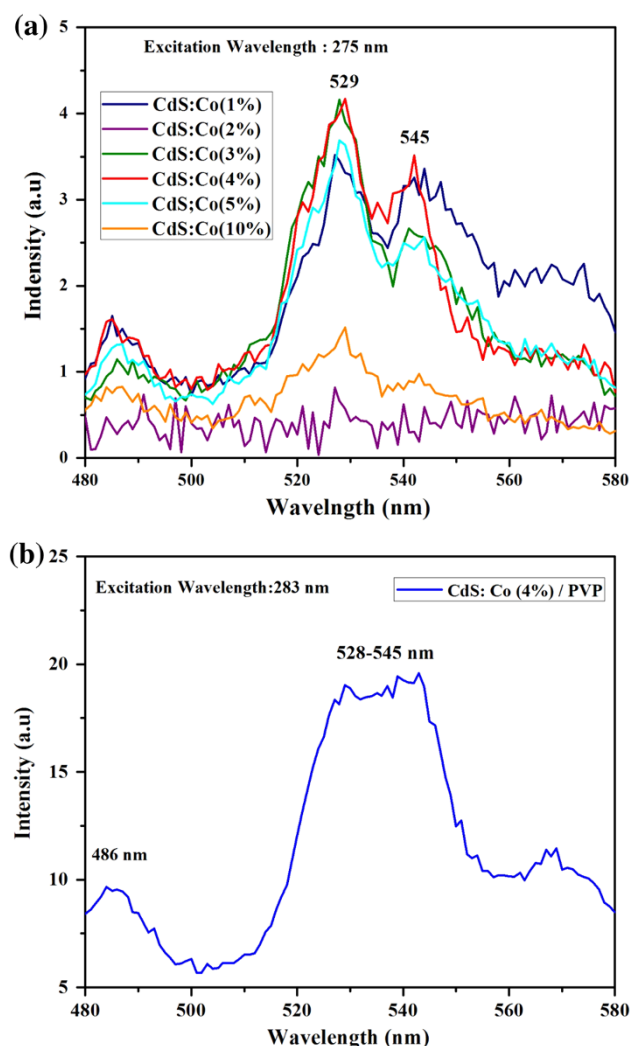


**Fig. 5** **a** Photoluminescence spectrum of the CdS:Co<sup>2+</sup> (1–5 and 10 %) nanoparticles (excitation wavelength = 275 nm), **b** PL spectrum of CdS:Co (4 %) with PVP-capped nanoparticles (excitation wavelength = 283 nm)

minimize the surface defects and enhance the electron–hole recombination (Paul and Nigel 2001). The present study indicates that the role of PVP is not only used to control the particle size but also reduce the surface defects of CdS (Fig. 5b).

#### Cyclic voltammetry (CV) studies

Figure 6a, b shows the CVs of CdS and CdS:Co nanoparticles on the glassy carbon with 0.1 M LiClO<sub>4</sub> supporting electrolyte at a constant scan rate of 20 mV s<sup>−1</sup>, respectively. As shown in Fig. 6a, three cathodic peaks (C1, C2 and C3) and one anodic (A1) peak have been observed at 0.60, −0.86, −1.34 and −0.68 V, respectively. Among them C1, corresponding to the reduction of CdS nanoparticle, appears as a modified electrode with CdS:Co

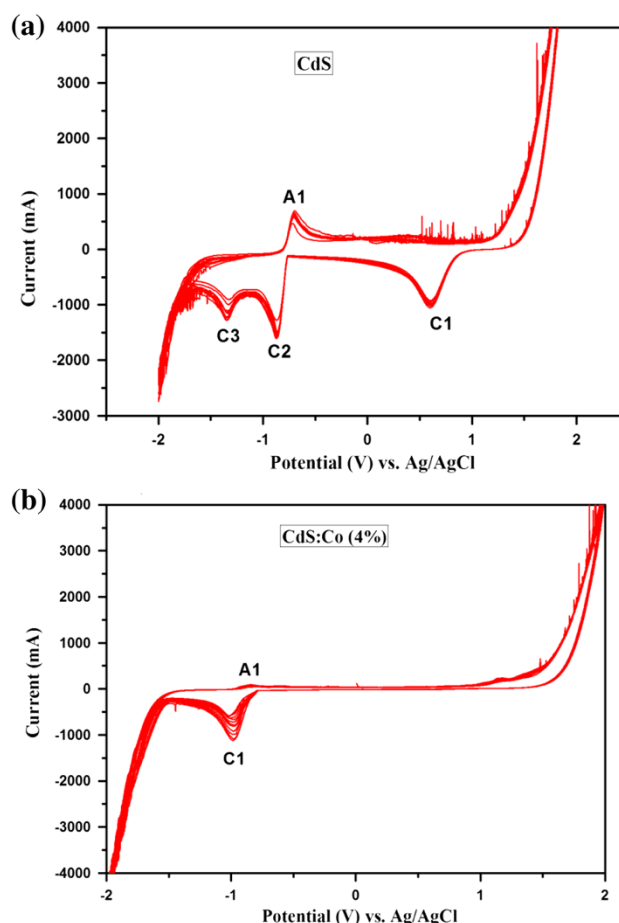


**Fig. 6** **a, b** CV curves of CdS and CdS:Co nanoparticles

nanoparticles (Fig. 6b). C2 and C3 have been attributed to the reduction of electrolyte. A1 is probably involved in the oxidation of OOH produced by dissolved oxygen (Cui et al. 2004). Figure 6b shows CV curves of CdS:Co nanoparticles which contain one cathodic peak at −0.98 V (C1) and one anodic peak at −0.86 V (A1). Compared to the two CV curves, CdS-modified electrode curves showed increasing peak areas with increasing peak current than Co-doped CdS. It dictates the increasing supercapacity behavior of the CdS.

#### EPR spectral analysis

Electron paramagnetic resonance (EPR) spectroscopy is a method for characterizing structure, dynamics and spatial distribution of paramagnetic ions. Due to the presence of at least one unpaired electron many paramagnetic species are chemically active. EPR spectroscopy is a valuable technique for obtaining detailed information on the geometric and electronic structure of various materials. Therefore, this technique is applied to study the nature of doped Co<sup>2+</sup> ions in the CdS lattice.

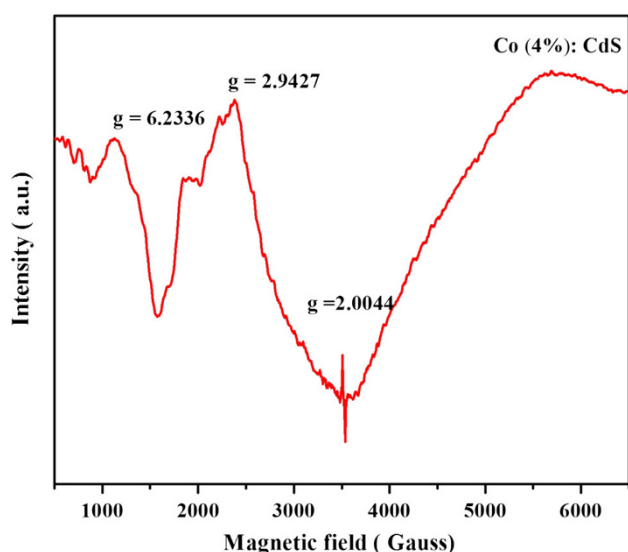


**Fig. 7** Room temperature ESR spectrum of free-surfactant 4 % Co:CdS nanoparticles

The EPR spectrum of the  $\text{Co}^{2+}$ -doped CdS nanoparticles is shown in Fig. 7.

$\text{Co}^{2+}$  ions ( $3d^7$  configuration with  $S = 3/2$ ,  $I = 7/2$ ) can appear both at high-spin ( $S = 3/2$ ) and at low-spin ( $S = 1/2$ ) configurations and have different characteristics in tetrahedral and octahedral coordination. EPR spectra and spin-Hamiltonian parameters are well understood for high-spin  $\text{Co}^{2+}$  in ideal high crystal field symmetries and at the tetragonal distortion (Bencini and Gatteschi 1982; Banci et al. 1982). The theory for octahedral field Oh predicts that the EPR spectrum is isotropic with  $g = 4.33$  (Abraham and Pryce 1951). This value markedly differs from true  $g$ -factors which are close to  $g = 2$ . This is due to considerable

excited orbital contributions and spin-orbit coupling. As a consequence, the  $g$ -values are extremely sensitive to the distortion of the octahedral environment and vary in the range  $g = 2$ –9.

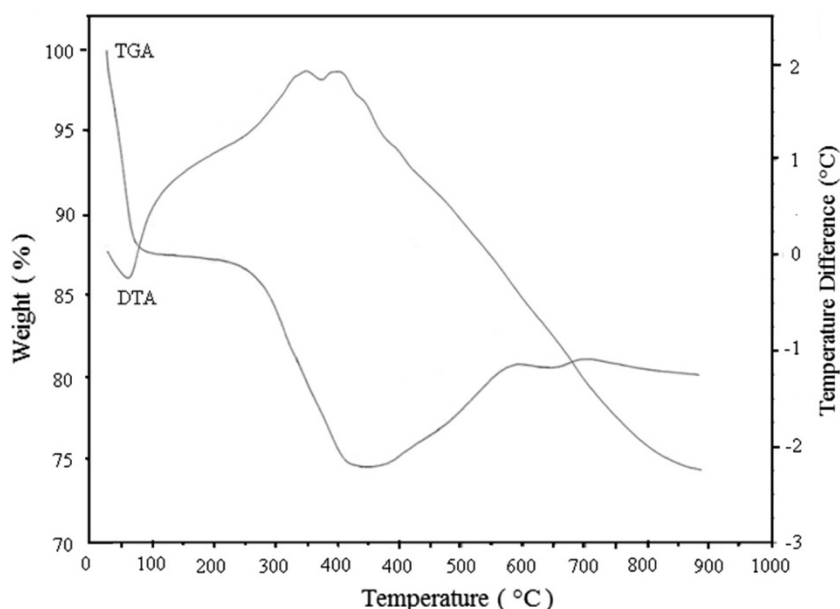
For high-spin  $\text{Co}^{2+}$  in the distorted tetrahedral geometry, either the  $\pm 1/2$  state or the  $\pm 3/2$  state can be lower in energy (Drulis et al. 1985; Pilbrow 1978). The  $\pm 1/2$  state is lower in a flattened tetrahedron, and the  $\pm 3/2$  state is lower in an elongated tetrahedron of  $D_{2d}$  symmetry. The true  $g$ -factors are expected in the range 2.2–2.4, whereas the  $g$ -factors for the effective spin  $S_0 = 1/2$  varies from 2 to 6.

The low-spin  $\text{Co}^{2+}$  complexes with  $S = 1/2$  often appear for the square planar and in pseudo-tetrahedral geometry (Jenkins et al. 2002), and they are easily distinguished from the high-spin complexes. The  $g$ -factors are in the range 1.5–3.3, and ground state strongly depends on the crystal field strength, geometry and mixing of configurations (Bencini and Gatteschi 1982; Daul et al. 1979). It is clear from the above that it is possible to distinguish between octahedral and tetrahedral complex geometry and the spin state of  $\text{Co}^{2+}$  considering the sum of the  $g$ -factors only.

#### TG–DTA study

Thermogravimetric analysis (TGA) and differential thermal analysis (DTA) have been used to study the thermal decomposition of  $\text{Co}^{2+}$ -doped CdS nanoparticles. The synthesized specimens were heated from room temperature to 800 °C with a heating rate of 20 °C  $\text{min}^{-1}$  in air atmosphere. Figure 8 shows the combined TG–DTA curves of 4 % Co:CdS nanoparticles. The observed mass loss of TGA curve up to 100 °C mainly corresponds to

**Fig. 8** TG and DSC curves of free-surfactant CdS:Co (4 %) nanoparticles



evaporation of water. In addition, the enormous mass loss around 260–400 °C indicates the removal of residual component and organic molecules. The strong exothermic peaks (DTA) at 347 and 399 °C are probably corresponding to the lattice deformation and the improvement of the crystallinity, respectively. Additionally, above 500 °C there is a smooth downward trend is observed in the DTA curve. This may be due to the release of sulfur ions from the sample. Further increase in the temperature from 500 to 700 °C leads to a significant mass gain on the TG curve, due to the oxidation.

## Conclusion

Co<sup>2+</sup> (1–5 and 10 %)-doped CdS nanoparticles were synthesized by the chemical precipitation method and their structural, optical and electrochemical properties were discussed. The broad XRD pattern of all the doped samples shows that the prepared particles were in the nanoscale range (6–14 nm) and that the synthesized rod-like structures of CdS:Co may be used for sensor applications. The doped Co<sup>2+</sup> ions entered in the host CdS lattice at both octahedral and tetrahedral coordinations without disturbing the hexagonal structure of CdS. Optical absorption and EPR spectra also confirmed that the doped Co<sup>2+</sup> ions occupied at octahedral and tetrahedral site symmetry. PL spectrum showed characteristic CdS emission bands in UV and blue regions. Optical absorption of all the doped samples was fairly blue shifted from the bulk CdS due to the quantum confinement effect. Thermal stability dopant and phase change were identified by TG–DTA analysis. The well-structured, electrochemical and optical material might be effectively used in some optoelectronic-related fields, for example photocatalytic and photovoltaic devices.

**Acknowledgments** The author would like to acknowledge the service rendered by CECRI, Karaikudi, Tamilnadu, India, for XRD, UV–Visible, PL, TEM, EPR, TG–DTA studies and CISR, Annamalai University, for recording FT-IR spectra. I would like to gratefully thank Dr. R. Gokul Krishnan, Chairman, Meenakshi Ammal Trust, Chennai, for support.

**Open Access** This article is distributed under the terms of the Creative Commons Attribution License which permits any use, distribution, and reproduction in any medium, provided the original author(s) and the source are credited.

## References

Abraham A, Pryce MHL (1951) The theory of the nuclear hyperfine structure of paramagnetic resonance spectra in the copper Tutton salts. *Proc R Soc (Lond) A* 206:173–191

- Affy HH, Battisha IK (2000) Oxygen interaction with CdS based gas sensors by varying different preparation parameters. *J Mater Sci Mater Electron* 11:373–377
- Alivisatos AP (1996) Semiconductor clusters, nanocrystals, and quantum dots. *Science* 271:933–937
- Banci L, Bencini A, Benelli C, Gatteschi D, Zanchini C (1982) Structures versus special properties. *Struct Bond (Berl)* 52:38–86
- Bencini A, Gatteschi D (1982) The effect of antisymmetric exchange on the EPR spectra of coupled pairs of transition metal ions. *Mol Phys* 47:161–169
- Brus LE (1984) Electron–electron and electron–hole interactions in small semiconductor crystallites: the size dependence of the lowest excited electronic state. *J Chem Phys* 80:4403–4409
- Brus LE (1986) Electronic wave functions in semiconductor clusters: experiment and theory. *J Phys Chem* 90:2555–2560
- Cui H, Xu Y, Zhang ZF (2004) Multi-channel electrochemiluminescence of luminal in neutral and aqueous solutions on a gold nanoparticles self-assembled electrode. *Anal Chem* 76:4002–4010
- Daul C, Schlaepfer CW, von Zalewsky A (1979) The electronic structure of cobalt(II) complexes with schiff bases and related ligands. *Struct Bond (Berl)* 36:129–171
- Drulis H, Dyrek K, Hoffmann KP, Hoffmann SK, Weselucha-Birczynska A (1985) EPR spectra of low-symmetry tetrahedral high-spin cobalt(II) in a cinchoninium tetrachlorocobaltate(II) dihydrate single crystal. *Inorg Chem* 24:4009–4012
- Duan X, Huang FY, Agarwal R, Lieber CM (2003) Single-nanowire electrically driven lasers. *Nature* 421:241–245
- Frerichs R (1950) The cadmium sulfide X-ray detector. *J Appl Phys* 21:312–317
- Gopal A, Hoshino K, Kim S, Zhang X (2009) Multi-color colloidal quantum dot based light emitting diodes micropatterned on silicon hole transporting layers. *Nano Technol* 20(23):235201 (pp9)
- Hanif KM, Meulenberg RW, Strouse GF (2002) Magnetic ordering in doped Cd<sub>1-x</sub>Co<sub>x</sub>Se diluted magnetic quantum dots. *J Am Chem Soc* 124:11495–11502
- He T, Chen DR, Jiao XL, Wang YL, Duan YZ (2005) Solubility-controlled synthesis of high-quality Co<sub>3</sub>O<sub>4</sub> nanocrystals. *Chem Mater* 17:4023–4030
- Hikmet RAM, Talapin V, Weller H (2003) Study of conduction mechanism and electroluminescence in CdS/ZnS quantum dot composites. *J Appl Phys* 93:3509–3514
- Hu H, Zhang W (2006) Synthesis and properties of transition metals and rare-earth metals doped ZnS nanoparticles. *J Opt Mater* 28:536–550
- Huynh WV, Dittmer JJ, Alivisatos AP (2002) Hybrid nanorod–polymer solar cells. *Science* 295(5564):2425–2427
- Jenkins R, Snyder RL (1996) Introduction to X-ray powder diffraction. John Wiley & Sons, New York
- Jenkins DM, Di Bilio AJ, Allen MJ, Betley TA, Peters JC (2002) Elucidation of a low spin cobalt(II) system in a distorted tetrahedral geometry. *J Am Chem Soc* 124:15336–15350
- Kar S, Chaudhuri S (2006) Cadmium sulfide one-dimensional nanostructures: synthesis, characterization and application. *Synth React Inorg Met Org Nano Met Chem* 36:289–312
- Khanna PK, Gokhale RR, Subbarao VVVS, Singh N, Jun KW, Das BK (2005) Synthesis and optical properties of CdS/PVA nanocomposites. *Mater Chem Phys* 94:454–459
- Kumbhoikar N, Nikesh VV, Kshirsagar A, Mahamuni S (2000) Photophysical properties of ZnS nanoclusters. *J Appl Phys* 88:6260–6264
- Liu YK, Zapfen JA, Geng CY, Shan YY, Lee CS, Lifshitz Y, Lee ST (2004) High-quality CdS nanoribbons with lasing cavity. *Appl Phys Lett* 85:3241–3243



- Martin TP, Schaber H (1982) Matrix isolated II–VI molecules: sulfides of Mg, Ca, Sr, Zn and Cd. *Spectrochem Acta A* 38:655–660
- Meng C, Yi X, Chen HY, Qiao ZP, Zhu YJ, Qian YT (2000) Templated synthesis of CdS/PAN composite nanowires under ambient conditions. *J Colloid Interface Sci* 229:217–221
- Murugadoss G (2010) Synthesis and optical characterization of PVP and SHMP-encapsulated  $\text{Mn}^{2+}$ -doped ZnS nanocrystals. *J Lumin* 130:2207–2214
- Nanda J, Sapra S, Srama DD, Chandrasekharan N, Hodes G (2000) Size-selected zinc sulfide nanocrystallites: synthesis, structure, and optical studies. *Chem Mater* 12:1018–1024
- Ohde H, Ohde M, Bailey F, Kim H, Wai CM (2002) Water-in- $\text{CO}_2$  microemulsions as nanoreactors for synthesizing CdS and ZnS nanoparticles in supercritical  $\text{CO}_2$ . *Nano Lett* 2:721–724
- Oladeji IO, Chow L, Ferekides CS, Viswanathan V, Zhao Z (2000) Metal/CdTe/CdS/ $\text{Cd}_{1-x}\text{Zn}_x\text{S}/\text{TCO}/\text{glass}$ : a new CdTe thin film solar cell structure. *Sol Energy Mater Sol Cells* 61(2):203–211
- Paul OB, Nigel LP (2001) Nanocrystalline semiconductors: synthesis, properties and perspectives. *Chem Mater* 13:3843–3858
- Pilbrow JR (1978) Effective  $g$  values for  $S = 3/2$  and  $S = 5/2$ . *J Magn Reson* 31:479–490
- Rossetti R, Hull R, Gibson JM, Brus LE (1985) Excited electronic states and optical spectra of ZnS and CdS crystallites in the 15 to 50 Å size range: evolution from molecular to bulk semiconducting properties. *J Chem Phys* 82:552–559
- Saravanan L, Pandurangan A, Jayavel R (2011) Synthesis of cobalt-doped cadmium sulphide nanocrystals and their optical and magnetic properties. *J Nanoparticle Res* 13:1621–1628
- Sathyamoorthy R, Sudhagar P, Balerna A, Balasubramanian C, Bellucci S, Popov AI, Asokan K (2010) Surfactant-assisted synthesis of  $\text{Cd}_{1-x}\text{Co}_x\text{S}$  nanocluster alloys and their structural, optical and magnetic properties. *J Alloys Compd* 493:240–245
- Singhal S, Chawla AK, Gupta HO, Chandra R (2010) Influence of cobalt doping on the physical properties of  $\text{Zn}_{0.9}\text{Cd}_{0.1}\text{S}$  nanoparticles. *Nanoscale Res Lett* 5:323–331
- Souici AH, Kechouche N, Delaire JA, Remita H, Mostafavi M (2006) Radiolytic synthesis and optical properties of ultra-small stabilized ZnS nanoparticles. *Chem Phys Lett* 422:25–29
- Sun ZB, Dong XZ, Chen WQ, Shoji S, Duan XM, Kawata S (2008) Two- and three-dimensional micro/nanostructure patterning of CdS-polymer nanocomposites with a laser interference technique and in situ synthesis. *J Nanotechnol* 19(3):035610–035611
- Uda H, Sonomura H, Ikegami S (1997) Screen printed CdS/CdTe cells for visible-light-radiation sensor. *Meas Sci Technol* 8:86–91
- Wang C, Lp KM, Hark SK, Li Q (2005a) Structure control of CdS nanobelts and their luminescence properties. *J Appl Phys* 97:054303–054306
- Wang QQ, Zhao GL, Han GR, Wang QQ, Zhao GL, Han GR (2005b) Synthesis of single crystalline CdS nanorods by a PVP-assisted solvothermal method. *Mater Lett* 59:2625–2629
- Weller H (2003) Synthesis and self-assembly of colloidal nanoparticles. *Philos Trans R Soc A Math Phys Eng Sci* 361:229–240
- Xiao M, Wang CY, You M, Zhu YR, Chen ZY, Hu Y (2001) A novel ultraviolet-irradiation route to CdS nanocrystallites with different morphologies. *Mater Res Bull* 36:2277–2282